Atomistic modelling of crystal structures of Friedel's salts Ca<inf>2</inf>Al(OH)<inf>6</inf>(Cl,CO<inf>3</inf>,OH)·mH<inf>2</inf>O:

Cement and Concrete Research 191 (2025) 107821

Contents lists available at ScienceDirect

Cement and Concrete Research

journal homepage: www.elsevier.com/locate/cemconres

Atomistic modelling of crystal structures of Friedel's salts $Ca_2Al(OH)_6(Cl, CO_3,OH)\cdot mH_2O$: Its relation to chloride binding

Liming Huang [a,*], Erik Bialik [b,*], Arezou Babaahmadi [a,*]

[a] Department of Architecture and Civil Engineering, Chalmers University of Technology, 41296 Gothenburg, Sweden
[b] Molecules in Motion, Kvarnbyvallen 21, 43134 Mölndal, Sweden

ARTICLE INFO

Keywords:
Friedel's salts
AFm
Chloride binding
First principles computation

ABSTRACT

The diffusion of chloride critically affects the durability of reinforced concrete in exposure environments. Hydrocalumite-like (AFm) phases can bind chlorides to form Friedel's salts, retarding chloride ingress. However, the stability and structural parameters of Friedel's salts with mixed-anion interlayers are not fully understood. First principles computation was performed to provide the energy-minimum crystal structures for Friedel's salt and AFm phases with various substitutions and water contents. It shows that the mixing of Cl^- and OH^- significantly changes the lattice parameters. However, the mixing of $1/2CO_3^{2-}$ and Cl^- anion presents little effect on structural parameter. It is energetically favourable and hardly measurable by XRD but decreases chloride binding capacity. The interlayer hydroxide ions show considerable flexibility in terms of occupied sites, which may be a key factor for the stability of AFm phases. The modelling results align with the the structural changes of Friedel's salts reported in previous experiments.

1. Introduction

Cementitious construction materials are durable when utilized in normal conditions, but due to their intrinsically weak tensile strength and cracking sensitivity they require steel reinforcement in most applications as structural concrete. The hydrated cementitious matrix is porous, which makes the steel reinforcements vulnerable to the ingress of aggressive ions from the exposure environment. In particular, chlorides from seawater or de-icing salts can initiate corrosion, which is one of the most frequent causes of degradation in structural construction materials [1,2]. Therefore, the mechanism of chloride ingress is an important research topic for durability design of sustainable concrete. Transport of chloride ions in the pores of hydrated cementitious materials is a coupled diffusion-binding process. The concentration gradients between the surrounding solution and the pore solution drives chloride ions inward. Some of the chloride ions are incorporated into hydration products in the cementitious matrix through chemical binding and some are absorbed on particle surfaces, i.e., physically bound. It is desirable to formulate concretes to maximize binding by either type of mechanisms. With incorporation of supplementary cementitious materials (SCMs) one can expect varying hydrate phase assemblage, pore solution composition and consequently pH levels depending on the type, amount, and reactivity level of the utilized SCM [3–5]. There has been much discussion on different possibilities for the chemical binding in cementitious systems in ettringite, AFm as well as calcium alumino-silicate hydrates (CASH); the state-of-the-art research implies that neither ettringite nor C-A-S-H accounts for the chemical binding of chlorides, and only AFm phases take part in chemical binding [6].

The general formula of an AFm phase is $[Ca_2(Al,Fe)(OH)_6]\cdot Y\cdot xH_2O$, where Y represents a monovalent anion or 0.5 of a divalent anion and x is the number of water molecules. AFm phases have a crystalline layered structure with a positively charged main layer, $[Ca_2Al(OH)_6]^+$, where portion of of Al^{3+} can be replaced by Fe^{3+} [7]. The resulting charge is compensated by the Y anions, which occupy space between the cationic layers together with the water molecules [8,9]. Several previous work proposed that interlayer anions can be substituted for one another [10–12]. In particular, sulfate- or carbonate-containing AFm phases can transform into a chloride-containing phase known as Friedel's salt (FS), $[Ca_2Al\ (OH)_6]\ Cl\cdot 2H_2O$, and thus sequester chloride ions [13], The low-temperature stable structure (< 34–$35\ ^\circ C$ [14,15]) is illustrated in Fig. 1. Such a pure-chloride phase is, however, an idealization. More typical are solid solutions with more than one species of anion in the interlayer. For the most relevant anions that would influence the chloride binding of AFm phases, there would be putative ternary solid solutions forming

* Corresponding author.
E-mail address: limingh@chalmers.se (L. Huang).

https://doi.org/10.1016/j.cemconres.2025.107821
Received 23 October 2024; Received in revised form 4 January 2025; Accepted 4 February 2025
Available online 14 February 2025

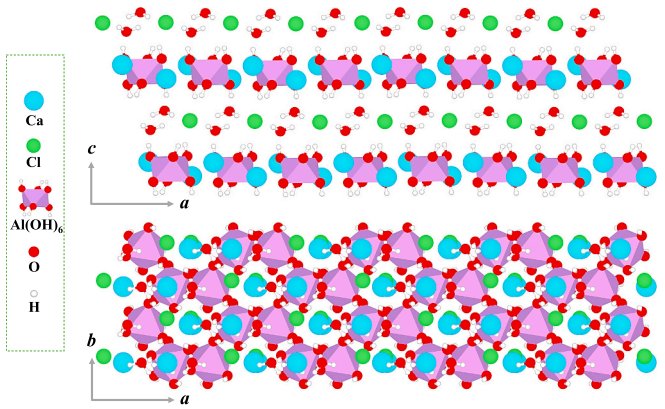

Fig. 1. Crystal structure of chloride-rich Friedel's salt. Bonds between Al and O are drawn in polyhedron to show the octagonal coordination.

between SO_4^{2-}, CO_3^{2-} and OH^-, as well as Cl^-, OH^-, CO_3^{2-} and even formate anions are known to exist in AFm phases and their phase assemblage depends on the temperature and pH of the environment [10,11,16]. However, there is no clear understanding of how the mixing of interlayer ions alters the crystal structure of these phases. This causes challenges for building a correct quantitative model for description of chemical chloride binding in modern concretes.

Several analytical techniques, e.g. Nuclear magnetic resonance, in-situ and synchrotron x-ray diffraction, have been employed to characterize and understand the structure of FS [6,14,15,17]. The octahedral coordination of aluminum in the structure of FS is distinguishable from the tetrahedral coordination in AFt phases by ^{27}Al Solid State NMR Spectroscopy. The previous investigations stated that XRD provided crystallographic information that is useful for distinguishing FS from other AFm phases, particularly the basal spacing between planes. Accurate quantitative measurements are possible using synchrotron radiation [14,17,18]. However, the interlayer structure of FS and AFm phases is affected by several factors, including the anion types and the moisture content. Georget et al. [19] demonstrated that the basal spacing of the hemicarbonate-Friedel's salt solid solution can be used to calculate its stoichiometry only when measured in wet conditions.

The effect of pH on chloride content of the FS had not been quantified in the literature until recently. According to a study by Hemstad et al. [20] and reported results by Avet and Scrivener [21], the chloride content of the FS, is influenced by the pH, and the actual phase almost never has a composition close to the ideal FS stoichiometry. The structure and composition of AFm phases are interrelated in subtle ways. Wilson et al. [22] concluded that the correlation between the chloride content of the Friedel's salt solid solution and the water-soluble chloride content suggests a dependence on several factors. These include the chloride contents in the exposure solution, the presence of competing ions like HO^- and SO_4^{2-}, the C-A-S-H content, and its reversible binding capacity within the pore solution. This highlights the strong dependence of FS chloride content on the surrounding pore solution conditions. Moreover, minor structural differences in the crystals of AFm phases can significantly affect their chemical binding capacity during the phase transition to FS, but these changes are difficult to detect using XRD. These discoveries have revealed a huge knowledge gap in the area of chloride binding in cementitious materials. Some previous investigation proposed new "proof-of-concepts" models for two of the solid solutions (CO_3-SO_4-OH AFm and CO_3-Cl-OH) [19]. In addition to gathering more solubility data, it also requires detailed information of the crystal structure with correct description of the interactions between water, chloride and carbonates in the AFm interlayer.

In this study, first-principles computations were carried out by optimizing the electronic structure to investigate the effect of ion substitutions on the local structure of the Friedel's salt (FS) interlayer. The primary focus is on the mixed interlayer ion system, exploring the atomistic structure of Friedel's salt and AFm phases with different combinations of carbonate, chloride, and hydroxide ions, as well as varying water contents. The implications of these findings for chloride binding, particularly in relation to carbonate and hydroxide substitutions, will be discussed and compared with previously reported experimental data from literature. These insights enhance the understanding and quantification of chloride binding in low-carbon binder systems, supporting the design of more durable cementitious materials.

2. First principles computation

2.1. Electronic structure calculations

All atomic positions along with the unit cell parameters were optimized using the Broyden–Fletcher–Goldfarb–Shanno (BFGS) algorithm [23] to give a minimum energy structure. The crystal system, however, was not allowed to change during optimization. The convergence criteria for structure optimization were that the maximum atomic displacement was 0.003 a_0 and that the maximum force on any atom was 0.00045 E_h/a_0, as well as that the root mean square value of these quantities were <0.0015 a_0 and 0.0003 E_h/a_0, respectively. The pressure tolerance in the cell optimization was 100 bar. In cases where arbitrary modifications were done to the composition and/or structure to create a starting guess for the structure, a constrained minimization with fixed unit cell parameters was always carried out before the full minimization. The energy of the periodic system was calculated using Kohn-Sham density functional theory using the Perdew-Burke-Ernzerhof (PBE) exchange-correlation functional in the Generalized Gradient Approximation (GGA) framework with the D3 dispersion correction scheme applied to all non-cation atoms [24,25]. Following [26], which argues that metal cations have such low polarizability that their dispersion interactions are negligible, no dispersion correction was applied for atom pairs that include a metal cation. A hybrid Gaussian and plane wave basis set was used with the TZVP-MOLOPT-PBE basis set for the Gaussian part and a plane wave cut-off of 300 Ry. Only valence electrons were represented explicitly; core electrons were replaced by Goedecker-Teter-Hutter (GTH) pseudopotentials [27]. The Quickstep module of the CP2K program package, version 9.1, was used for all calculations. This code is highly optimized for rapid calculations in condensed phases [28].

2.2. System compositions and starting structures

The focus of this work is coexistence of different anions within the same interlayer, instead of completely alternative layers such as Kuzel salt or U-phase [9,29,30]. Therefore, the Friedel's salt was selected as a starting structure for mixing ions interlayers. We determined the minimum energy structures of FS with composition variations summarized in Table 1. The structures considered here are hypothetical compounds

Table 1
Summary of ion substitutions considered for FS and abbreviations.

Abbreviations	Interlayer composition
FS(10)	$Cl^-{\cdot}2H_2O$
OH-AFm(11)	$OH^-{\cdot}2H_2O$
Cl-OH-AFm(10.5)	$0.5Cl^-{\cdot}0.5OH^-$ $2H_2O$
OH-AFm(13)	$OH^-{\cdot}3H_2O$
Cl-OH-AFm(11.5)	$0.5Cl^-{\cdot}0.5OH^-$ $2.5H_2O$
Monocarbonate(11)	$0.5CO_3{\cdot}2.5H_2O$
Cl-CO_3-AFm(10)	$0.5Cl^-{\cdot}0.25CO_3^{2-}{\cdot}2H_2O$
Cl-CO_3-AFm(10.5)	$0.5Cl^-{\cdot}0.25CO_3^{2-}{\cdot}2.25H_2O$
Na-FS(10)	$0.5Cl^-{\cdot}2H_2O$
Na-FS(11)	$0.5Cl^-{\cdot}2.5H_2O$
Na-FS(12)	$0.5Cl^-{\cdot}3H_2O$

Note: numbers in parentheses represent the chemical bound water amount.

that may be conceptualized as purified defects in the FS structure, though they may share their stoichiometry with a known phase. This is the case for the hydroxide and hydroxide-water substitutions, which give the same stoichiometries as OH-AFm(11) and OH-AFm(13). When deemed necessary, additional starting structures were tried to check for the existence of lower-lying local minima than those previously found. Note that no systematic way to ensure that the minimum global energy is found in a high-dimensional system; the minimum energy structure reported is in all cases the structure corresponding to the lowest known energy. The total energy (E_t) of crystal structures is calculated with Eq. (1).

$$E_t = E_o + E_s + E_c + E_h + E_e + E_d \quad (1)$$

where E_o is overlap energy of the core charge distribution, E_s is self-energy of the core charge distribution, E_c is core Hamiltonian energy, E_h is Hartree energy, E_e is exchange-correlation energy, and E_d is dispersion energy.

It is important to note that the minimum-energy structure only approximates the true structure at a temperature. Friedel's salt exists in a low-temperature and a high-temperature form, with the transition between them at about 35 °C [14,15]. While the two forms have different symmetries, the molecular-level structure is quite similar: In the high temperature form, each chloride ion is surrounded symmetrically by six water molecules, each of which also coordinates a Ca^{2+} ion. In the low-temperature form, this symmetry is broken such that the anion sits off-center in the distorted hexagon formed by the water molecules. Presumably, the phase transition is driven by the increasing importance of the entropy of the hydrogen bond network in the symmetric structure with higher temperature, where the symmetry allows a multitude of possible donor-acceptor patterns for the same overall connectivity. At some temperature, this contribution to the free energy comes to dominate the energetic gain from having a closer optimal hydrogen bonding geometry in the asymmetric structure. As the system's free energy (relative to some standard state) is orders of magnitude more costly to compute than the system energy, we focus on the energy-dominated low temperature form in this study. As the structural differences between the low- and high-temperature forms are modest, we expect that the broad conclusions can be generalized to the high-temperature form.

The XRD patterns of optimized structure were computed with Materials Studio under Reflex function- power diffraction mode with structure of primitive cell provided in Table 2. The radiation source was set as Cu Kα2 (λ = 1.544 Å).

3. Results

3.1. The optimized structure of Friedel's salt

The crystal cell information of the optimized structure is summarized in Table 2, and Fig. 2 shows the interlayer features of corresponding structures. Detailed information of atomic coordination for each structure is provided in the supplementary information (SI) as *xyz* files. The computed energy-minimum structure is very close to the low-temperature FS characterized by synchrotron powder diffraction [C2/c; a = 9.960(4) Å, b = 5.7320(2) Å, c = 16.268(7) Å, β = 104.471(2)°] [14]. The calculated values for |**a**| and |**b**| are overestimated by a few percentages compared to the experimental values. This probably reflects the intrinsic error of the electronic structure method, which is known to overestimate bond lengths and ion sizes [31]. The value of |**c**|, that corresponds to the basal spacing, is remarkably close to the experimental value. The simulated 2θ value of the layer structure (plane (002)) is 11.26°, which is also almost the same as experimental value with 11.22°.

Cl-OH-AFm (10.5) has an interlayer structure with the substitution of half chloride ions by hydroxide ions. The crystal structure reaches the minimum energy when the hydroxide stays in the same site as chloride (see Fig. 2). A full substitution of interlayer chloride with hydroxide forms OH-AFm(11) also has the minimum energy with anions in the same sites. The hydroxide substitution seems to have little influence on |**a**| and |**b**|; however, it decreases the |**c**| of the cell. This appears to be due to the smaller size of the hydroxide ion than the chloride ion. For the same reason the hydroxide ions sit even further off-center than chloride in the ion binding site. The ability to form mixed phases depends on the interaction energy between adjacent ions. Therefore, the 'mixing energy' to form the half hydroxide substituted system can be calculated by E[Cl-OH-AFm(10.5)] – (E[Friedel's salt] + E[OH-AFm(11)]). The energy change is found to be +20.8 kJ/mol, so it implies that the formation of the mixed phase from the pure ones is energetically unfavorable.

In the half carbonate substituted FS structure, Cl-CO_3-AFm(10), the carbonate ion fits well within the empty chloride site and accepts six hydrogen bonds from adjacent water molecules. In each of these H-bond interactions the O–O distance is between 2.5 and 2.7 Å, which is a little shorter than the O–O distance measured in liquid water [32,33]. The two water molecules that would form hydrogen bonds in the empty ion site and hydrogen bond to the carbonate ions. This empty ion site can easily accommodate the extra water molecule. The unit cell parameters are remarkably similar to the experimental value [12,34], which is also very close to values for unmodified FS, allowing for the fact that the unit cell for the carbonate substituted structures corresponds to two primitive cells in the FS structure. Most part of modelled XRD pattern for these two structures looks very similar, but some new peaks can be observed in 2θ range of 8–10° and 30–36° for Cl-CO_3-AFm(10) as shown in Fig. 2. This is similar to the finding of new peaks caused by secondary interlayer ions from some recent modelling by Honorio [35]. For the full substitution of chloride with carbonate ions, Monocarbonate(11), the interlayer distance is similar to that for the half-carbonate substitutions, but the hydrogen bonding situation is somewhat changed. There is no possible arrangement that places the carbonate ions further apart while keeping the FS structure, though there is almost certainly a considerable energetic cost associated with divalent carbonate ions being so close together. The diffraction peak of plane (002) only has about 0.2°

Table 2
Information of optimized unit cell parameters for anions substitution in Friedel's salts.

Abbreviations	Chemical formula	Cell volume/Å^3	Density g/cm^3	Crystal parameters					
				a (Å)	b (Å)	c (Å)	α (°)	β (°)	γ (°)
FS (10)	$Ca_4Al_2Cl_2(OH)_{12}(H_2O)_4$	930.29	2.00	10.11	5.87	16.21	90	104.86	90
Cl-OH-AFm (10.5)	$Ca_4Al_2Cl(OH)_{13}(H_2O)_4$	910.46	1.98	10.03	5.90	15.93	90	105.21	90
OH-AFm (11)	$Ca_4Al_2(OH)_{14}(H_2O)_4$	880.73	1.98	10.08	5.89	15.37	90	105.08	90
OH-AFm (13)	$Ca_4Al_2(OH)_{14}(H_2O)_6$	935.38	1.99	10.03	6.02	16.09	90	105.53	90
OH-AFm (13) he*	$Ca_4Al_2(OH)_{14}(H_2O)_6$	929.44	2.00	9.97	6.03	16.04	90	105.61	90
Cl-OH-AFm (11.5)	$Ca_4Al_2Cl(OH)_{13}(H_2O)_5$	929.33	2.00	10.07	5.96	16.02	90	105.07	90
Cl-OH-AFm (11.5) he*	$Ca_4Al_2Cl(OH)_{13}(H_2O)_5$	920.12	2.02	10.06	5.94	15.94	90	104.99	90
Monocarbonate (11)	$Ca_4Al_2CO_3(OH)_{12}(H_2O)_5$	1869.92	1.95	10.20	11.68	16.15	90	103.60	90
Cl-CO_3-AFm (10)	$Ca_4Al_2Cl(CO_3)_{0.5}(OH)_{12}(H_2O)_4$	1870.29	1.97	10.13	11.71	16.26	90	104.07	90
Cl-CO_3-AFm (10.5)	$Ca_4Al_2Cl(CO_3)_{0.5}(OH)_{12}(H_2O)_{4.5}$	1875.90	2.00	10.10	11.72	16.33	90	103.84	90

Note: he* represents a crystal structure with a bit higher total energy.

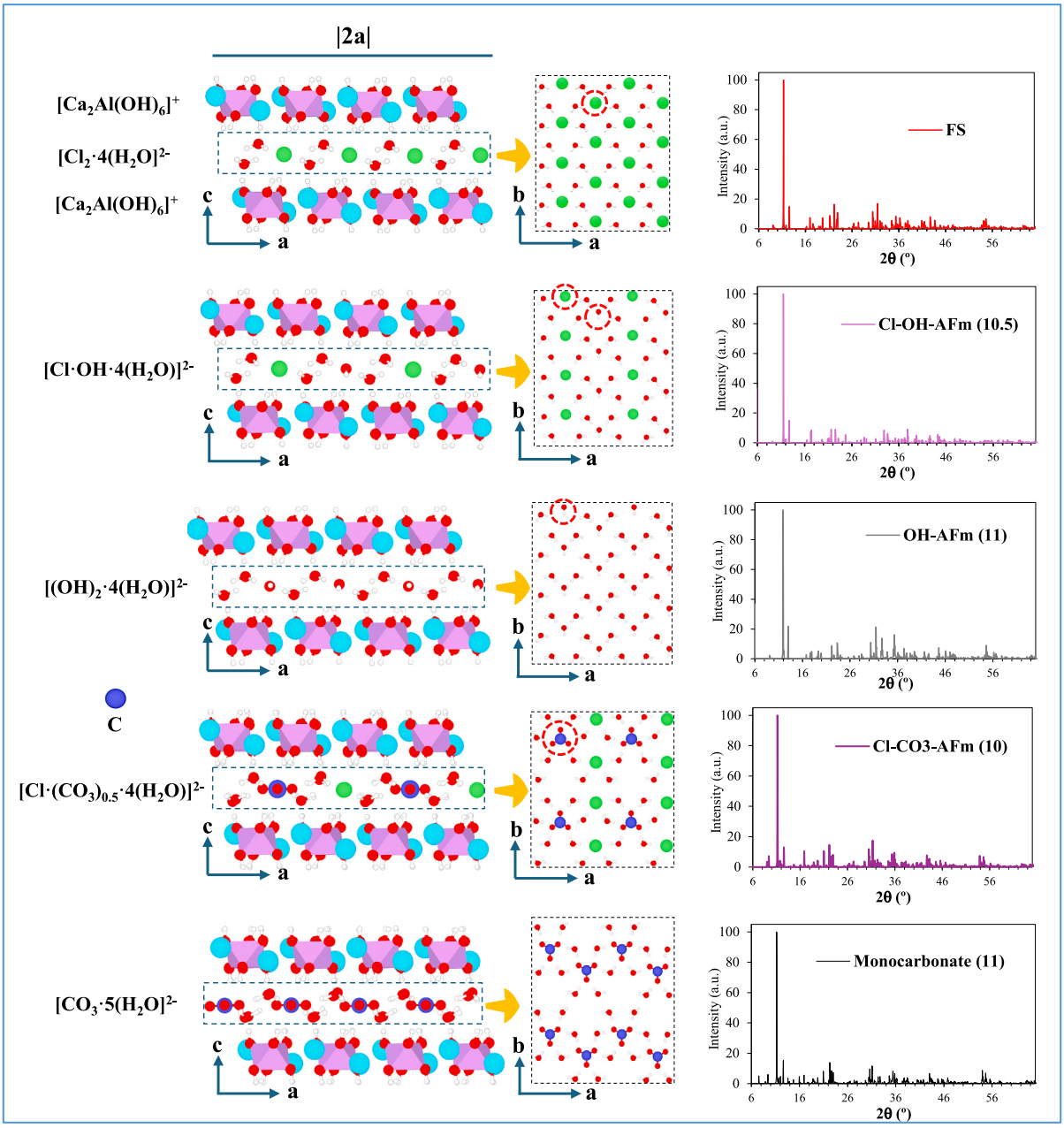

Fig. 2. Illustration of the energy minimum structure with different cation substitutions and the modelled XRD patterns, and the red circle marks the site with replacement of various anions. (For interpretation of the references to colour in this figure legend, the reader is referred to the web version of this article.)

difference in 2θ of Cl-CO_3-AFm(10) and FS structure, which can barely be detected by normal XRD test. The adsorption of one more water molecule in structure will lower the energy of Cl-CO_3-AFm. As shown in Fig. 3, the mixing energy of Cl-CO_3-AFm(10.5) can be calculated and the value is −27.5 kJ/mol. The negative energy value implies that this kind of transformation is energetically preferable. The effect of interlayer water numbers on the crystal structure will be discussed in the next section.

3.2. Effect of interlayer water molecules

The dehydration of AFm phases will cause a change in the structure of solid solution, especially the interlayer configuration and space [17,19]. The AFm phases with different water molecule numbers are compared in Fig. 4 and the mixing reaction energy of the crystal structure is compiled in Fig. 3. An integration of induces an increase in the |**b**| and |**c**| of the cell parameters (see Table 1). The change of interlayer spacing causes a shift of diffraction peak from 11.9° to 11.4° as shown in Fig. 4. One more water in the interlayer of Cl-OH-AFm(11.5) will form a cell structure closer to FS with a lower total energy than Cl-OH-AFm (10.5). The mixing energy of FS and OH-AFm(13) to form Cl-OH-AFm (11.5) is 13.5 kJ/mol, which implies the chloride-hydroxide hybrid structure has a little higher energy than the separate pure ion structures. Comparing with Cl-OH-AFm(10.5), this transition is more energetically favourable. The difference in layer space of these two structures is very minor. The uptake of one more water in Cl-OH-AFm causes almost no changes in the cell structure, density and cell volume in comparison with FS. For the Cl-CO_3-AFm, the effect of adding 0.5 water in primitive cells is negligible for cell parameters, so an overlapping of diffraction peak can be observed in XRD patterns.

As shown in Fig. 5, for the hydroxide-water substitution, two structures with similar energy were found, with the difference being only

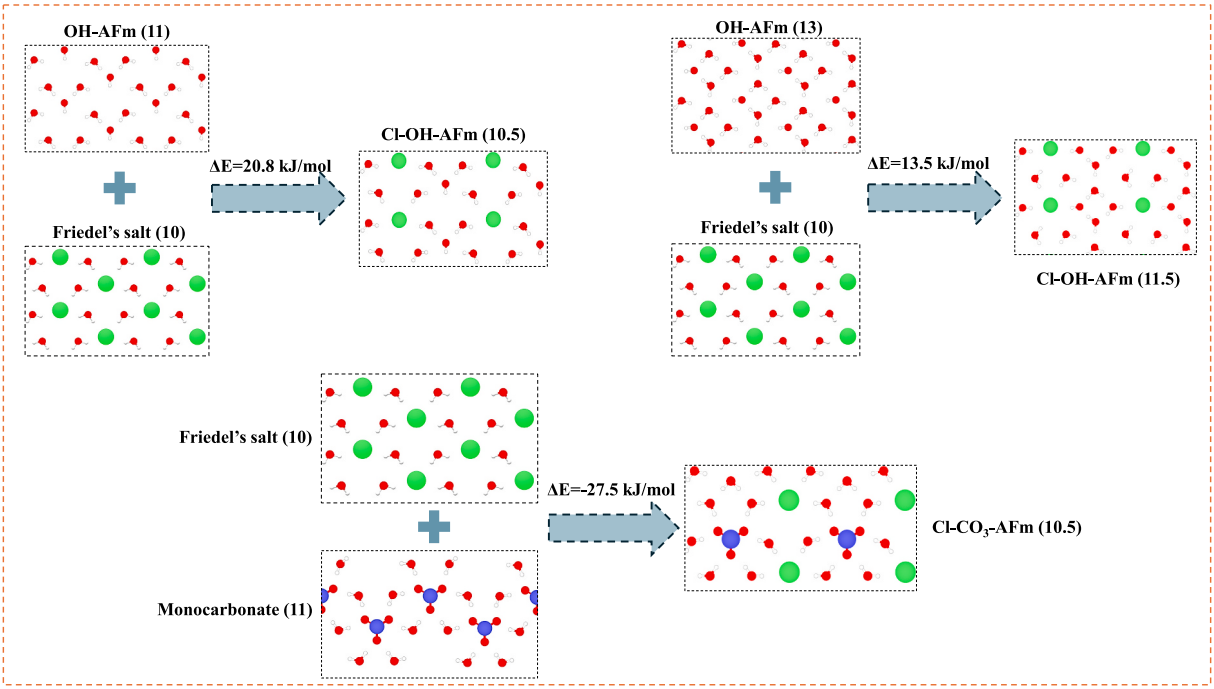

Fig. 3. Mixing energy of the optimized structure for AFm family with different interlayer anions.

6.66 kJ/mol per ion. In the higher energy structure, the ion is in the FS chloride site like in the hydroxide substituted structure. In the lower energy structure, the hydroxide ion is in a water site. The FS ions site is occupied by two water molecules, favorably positioned to form hydrogen bonds between themselves, to surrounding water molecules and to the hydroxide ion. Presumably, it is this favourable hydrogen bonding situation that stabilizes the hydroxide ions in the water sites. With more interlayer water, the structure with the hydroxide ions occupying water sites is still more energetically preferable than with the hydroxide ions in an ion site, but only by 1.59 kJ/mol per ion. It may thus be more accurate to describe the structure with a partial occupancy of both sites. The hydroxide ions get quite close to the chloride ions, which can be explained by the fact that the hydroxide ions coordinate calcium ions.

Table 3 shows the change of cell parameters of hemicarbonate in various hydration states compared with FS as the start structure. Two optimized structure were found for Hemicarbonate(12) that differed in energy by only 1.1 kJ/mol per ion substitution. As this difference is so small that one should expect a significant population of the higher-energy structure at equilibrium, both are discussed. The presence of several structures of similar energy points to a limitation of the current methodology where a single minimum is seen as representative of the structure. The case of hemicarbonate should be revisited with a method that allows for proper thermal averaging and the conclusions about hemiacarbonate must be seen as preliminary. The predicted XRD peaks positions of plane (002) are close to those for FS, see Table 3. Though there may be lower energy structures yet to be found that more closely correspond to the structure of the pure phases [19], this suggests that hemicarbonate-like structures incorporated into FS may not be readily detectable by powder XRD. This observation may also rationalize the finding that the XRD peaks of AFm changes only modestly down to a chloride fraction of 0.5 [36]. The mixing energy of forming hemicarbonate was calculated according to the assuming reaction: 1/4E[OH-AFm(13)] + 1/8E[Monocarbonate(11)] → 1/8E[Hemicarbonate(12)]. It turns out that this process is slightly exothermic with $\Delta_{mix}E = -2.4$ kJ/mol. As a complete exploration of the Hemicarbonate(12) configuration space may uncover even lower-lying energy minima, the thermodynamic driving force to form Hemicarbonate(12) from the "pure" phases may be even greater.

The interlayer structures for the various hemicarbonates are shown in Fig. 6. There is not enough water sites in the structure of Hemicarbonate(9) to create hydrogen bonding opportunities (HB) network. The HB displayed in figure is calculated based on a typical length of 2.74 Å [37]. Both hydroxide ions and the carbonate ions occupy HB sites in Hemicarbonate(10.5), but it is still not sufficient to build hydrogen bond networks to connect all water molecules. This is in close analogy to the situation of OH-AFm(11), in which the water content is insufficient to form a system-spanning hydrogen bonding network. In Hemicarbonate (12), both hydroxide ions occupy HB sites in the lower energy structure, but one hydroxide ion is in a calcium coordinate (CC) site in the higher energy structure. This illustrates that the site preference of hydroxide ions depends on the chemical environment, in particular the hydrogen bonding network. In both structures, the carbonate ion was found in a HB site as expected from the calculations for Monocarbonate(11). Structures where the carbonate ion occupies a CC site were considered but invariably resulted in a much higher energy, implying a rather unstable structure.

3.3. Possible cation substitution with Na

Previous investigations found that pH had varying effects on the chemical binding of chloride in pastes, depending on whether calcium or sodium was present as the cation [19,22]. Sodium and calcium are similar in size but differ in charge. Substitution of Ca^{2+} with Na^{+} would thus change the charge balance such that one fewer chloride ion would be needed in the interlayer for each such substitution. We performed calculations where Ca^{2+} in one position was replaced by Na^{+} and the Cl^{-} ion nearest to the substitution site was deleted from the interlayer. While we expect that this corresponds to the lowest energy structure, we note that charge balance is satisfied regardless of which chloride ion is deleted. The deviations of the unit cell parameters from the starting structure are shown in Table 4.

The XRD diffraction peak of FS with Na cation substitution is presented in Fig. 7. One sodium substitution will cause an increase of the diffraction intensity in 2θ range of 9–10° and peak shifts in 2θ range of 20–25°, however the inclusion of one more water molecule in the

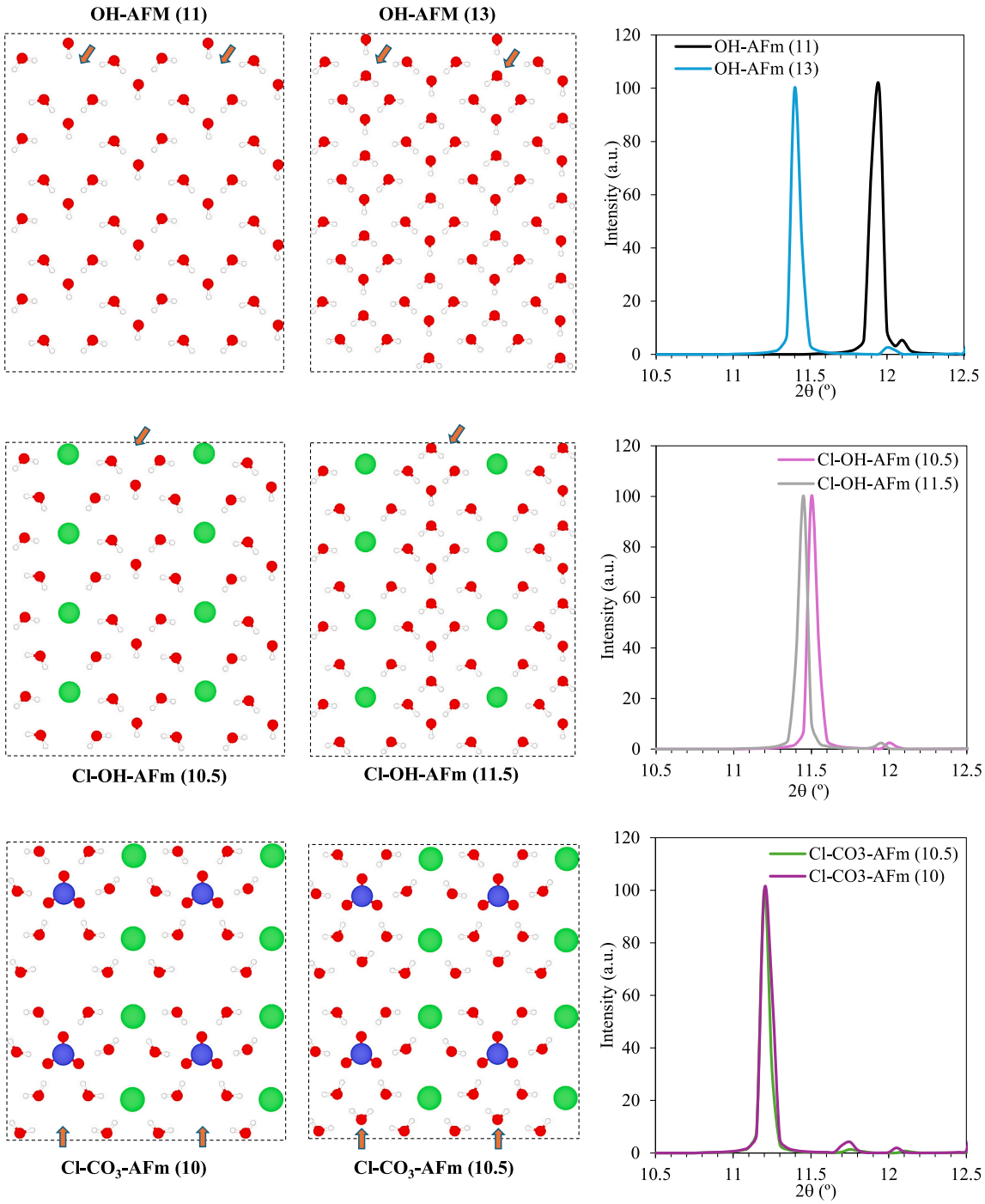

Fig. 4. The interlayer properties of AFm phases with various water amounts and the corresponding XRD peak of the layer structures.

structure makes all peaks similar to those of the original FS. Furthermore, two more water molecules in solid solution produce a structure with a stronger diffraction in 2θ range of 20–35°. These features may be useful for identifying the Na-FS in later experimental studies. Although there are no existing experimental results in literature that reported on the occurrence of sodium substituted FS structure, as sodium ions are similar in size to calcium ions, it seems plausible that sodium ions may substitute calcium ions in the crystal lattice. This is relevant to chloride binding as this substitution would decrease the need for chloride ions in the interlayer to neutralize the positive charge of the Al-Ca-OH layers. A further experimental investigation of the pure phase is meaningful to verify this modelling result.

Table 4 shows that the substitution of Ca by Na with different interlayer water numbers induces only minor deviations in the **a** and **b** vectors compared to the starting structure of FS. The **c** vector, corresponding to XRD of $2\theta_{(002)}$, however, does vary between these compositions. A substitution of Na gives a positive shift in 2θ of approximately 0.21°. The Na-FS (11) shows a negative shift, while the substitution of Na + $2H_2O$ to form Na-FS (12) shows practically no effects on the peak position. Thus, Ca–Na substitutions may go unnoticed if XRD is the only technique employed.

For analysing the water structure at the interlayer, the Na-substituted Al-Ca-OH layer of the minimum energy structure for the Na + H_2O, Na-FS(11), is shown in Fig. 8. The average distance from the sodium ion to the six nearest-neighbor oxygen atoms is 2.48 Å. This value is similar to the typical sodium-oxygen distance in aqueous

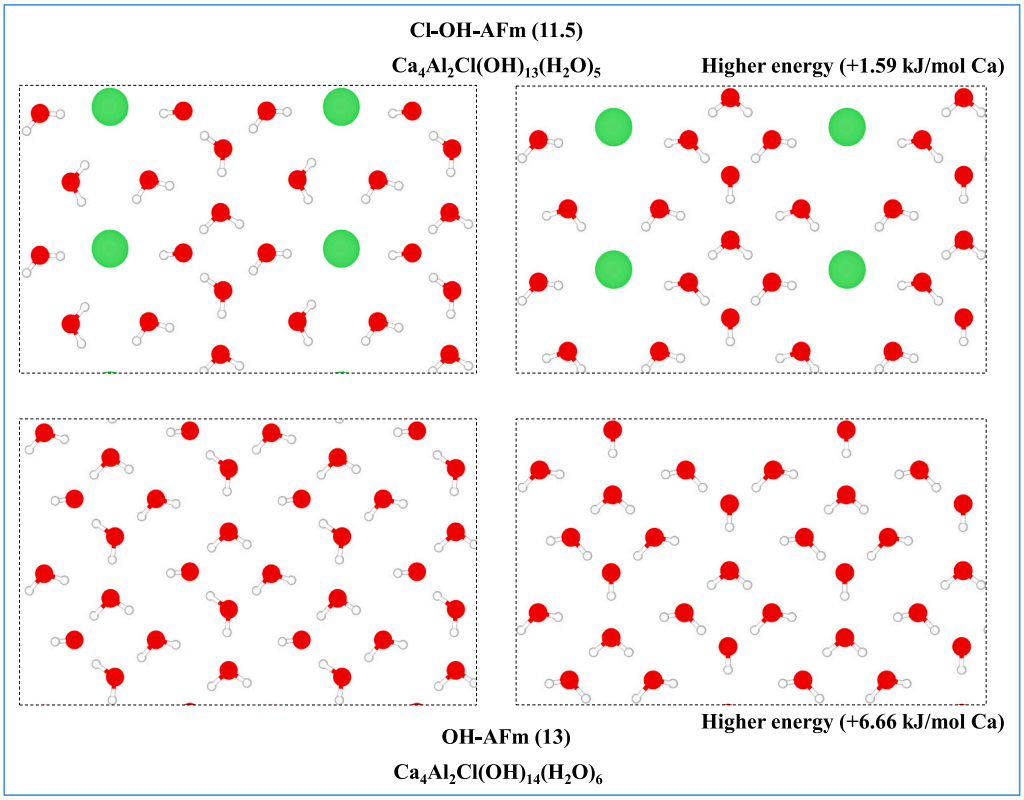

Fig. 5. Two configurations of hydroxide in Cl-OH-AFm and OH-AFm with minor difference in energy states.

Table 3
Summary of the simulated hemicarbonates and the change of structural parameters.

Abbreviations	Chemical formula	Change of cell parameters				$\Delta 2\theta_{(002)}$
		Δa (Å)	Δb (Å)	Δc (Å)	$\Delta\beta$ (°)	
Hemicarbonate(9)	$Ca_4Al_2(CO_3)_{0.5}(OH)_{13}(H_2O)_{2.5}$	−0.01	−0.09	−0.47	0.97	0.39
Hemicarbonate(10.5)	$Ca_4Al_2(CO_3)_{0.5}(OH)_{13}(H_2O)_4$	−0.04	−0.04	−0.06	0.51	0.07
Hemicarbonate(12)	$Ca_4Al_2(CO_3)_{0.5}(OH)_{13}(H_2O)_{5.5}$	−0.01	0.00	−0.08	0.52	0.08
Cl-CO_3-AFm (10.5)	$Ca_4Al_2Cl(CO_3)_{0.5}(OH)_{12}(H_2O)_{4.5}$	0.02	−0.03	−0.03	−0.26	0.03

solution, 2.43 Å, computed with a similar methodology [26], which is slightly larger than the experimental value of 2.38 Å [38]. The corresponding distance for the calcium ions is 2.45 Å in the minimum energy structure of Na-FS (11) and 2.44 Å in the starting structure. Thus, the calculations support the supposition that the ionic radii of sodium and calcium are sufficiently similar that one can replace the other with a minimal introduction of strain into the crystal lattice. The Al – O distances adjacent to sodium ions are a few hundredths of an Å shorter than those adjacent to only calcium ions. However, because nuclear magnetic resonance (NMR) spectroscopy is a sensitive reporter of chemical structure, this may be relevant to the small chemical shift differences between AFm exposed to NaCl and $CaCl_2$ solutions, as shown in Fig. 5 of previously reported work [39].

4. Discussion

In the pursuit of more sustainable concrete, modern binders will incorporate higher amounts of SCMs and limestone in composite binders such as limestone calcined clay cement or other ternary systems with incorporation of slag. The use of SCMs and limestone will not only modify the Al availability in the binder system to influence the phase composition of CASH and AFm phases [39–41], but more importantly for this research, it will alter the structure of AFm phase which is crucial for the accurate design and prediction of chloride binding capacity in low-carbon concretes.

There is a consensus that chloride only has a weak physical interaction with CASH and is mainly reserved in the diffuse layer the colloidal surface, which means these chlorides can reversibly transform back into free chlorides under certain conditions [42]. In contrast, AFm has a strong chemical interaction with chloride usually presented in the form of chloride-rich AFm phases. However, this binding capacity is strongly influenced by the chemical environment of the pore solutions. Fig. 9 presents a summary of findings from various experimental studies conducted by other researchers on the effects of pH and exposure solution composition on the structure and chloride binding in the AFm phase. The curves depicted are not exact representations of the data but rather simulated peak positions, estimated in part through back calculations based on the data presented in previous studies. They are designed to enhance visualization and facilitate comparison between the different reported data sets (for the original data, please refer to the cited references). The data presented on the top part of the curve in red (Red series) are extracted from the study of Georget et al. [19], which depicts synthesized FS samples with varying chloride content. Synthesis is conducted with excess $Ca(OH)_2$, resulting in high pH across all produced systems. However, a slight decrease is noticeable in systems with higher chloride content. Peak positions indicate that FS samples with the highest chloride content (Cl/Al = 1) exhibit peak positions similar to those of high-temperature FS. As the Cl/Al ratio decreases, the peaks

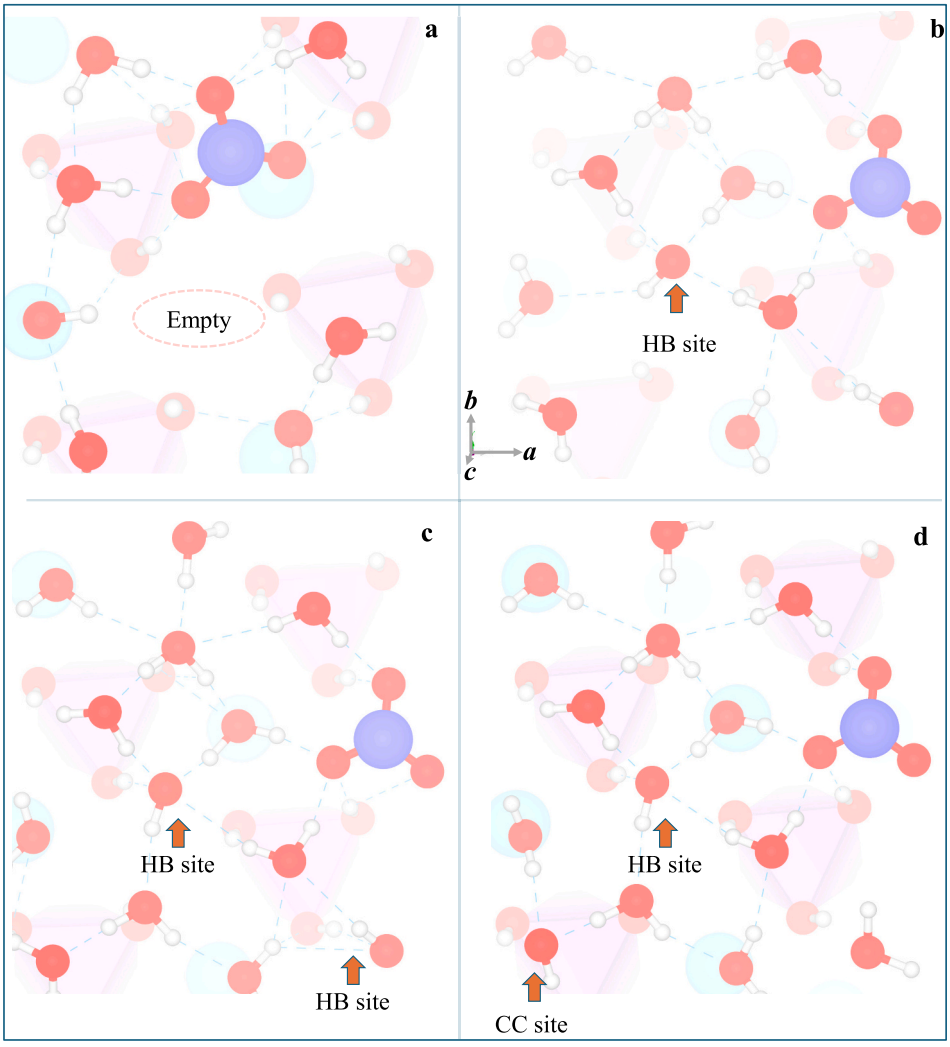

Fig. 6. Visualization of the interlayer in a) Hemicarbonate(9), b) Hemicarbonate(10.5), c) Hemicarbonate(12) (lower energy structure) and d) Hemicarbonate(12) (higher energy structure).

Table 4
Information of optimized unit cell parameters for possible cation substitution in FS.

Abbreviations	Chemical formula	Cell volume/Å^3	Density g/cm^3	Crystal parameters						$\Delta 2\theta_{(002)}$
				a (Å)	b (Å)	c (Å)	α (°)	β (°)	γ (°)	
Na-FS (10)	$Ca_3NaAl_2Cl(OH)_{12}(H_2O)_4$	919.09	1.84	10.18	5.85	15.96	90	104.90	90	0.21
Na-FS (11)	$Ca_3NaAl_2Cl(OH)_{12}(H_2O)_5$	940.84	1.86	10.12	5.86	16.41	90	104.78	90	−0.12
Na-FS (12)	$Ca_3NaAl_2Cl(OH)_{12}(H_2O)_6$	943.03	1.92	10.08	5.96	16.17	90	103.83	90	0.00

shift to higher diffraction angles, with a sharp decline in slope was observed between Cl/Al ratios of 0.5 and 0.25. However, aside from chloride concentration and the pH of the pore solution, Wilson et al. [22] found that the cation in solution also plays a pivotal role in mediating the formation of Friedel's salt (FS) in cementitious systems. Calcium ions serve as essential components of FS, providing anchoring sites for water molecules within the interlayer space, while aluminum contributes to its overall structure and stability.

As shown in Fig. 9, the increase of pH regulated by NaOH induces a decrease of Cl/Al in FS, and the shifts to lower diffraction angles, which is an inverse tendency in comparison with results from Georget et al. [19]. As demonstrated in Fig. 4, since the moisture state of the AFm phases affects the cell structure of the solid solution due to changes of hydrogen bond length in the layered structure, the differences in sample preparation are one of the important variables when comparing results from different studies. However, since Wilson et al. [22] and Georget et al. [19] used similar methods to dry their studied samples, the observed variations in peak positions cannot be solely attributed to moisture differences in the studied samples. Given that changes in chloride content alone should not influence interlayer spacing, other factors may be contributing to the variations. Even in high alkalinity condition, Appelo [43] concluded that pure OH-AFm is unstable and converts into hydrogarnet and portlandite, depending on the precipitation rate of hydrogarnet. The solubility of AFm is correlated with the charge of the anion, and inversely with the thickness of the anion-layer, in agreement with Coulomb's law. According to the mixing energy shown in Section 3.2, Cl-OH-AFm(11.5) is energetically stable in water-rich environments. The simulated peak shifts from ion substitution are summarized in Fig. 10. A substitution of Cl in FS by OH will push the peak of plan (002) toward a higher diffraction angle, which is consistent

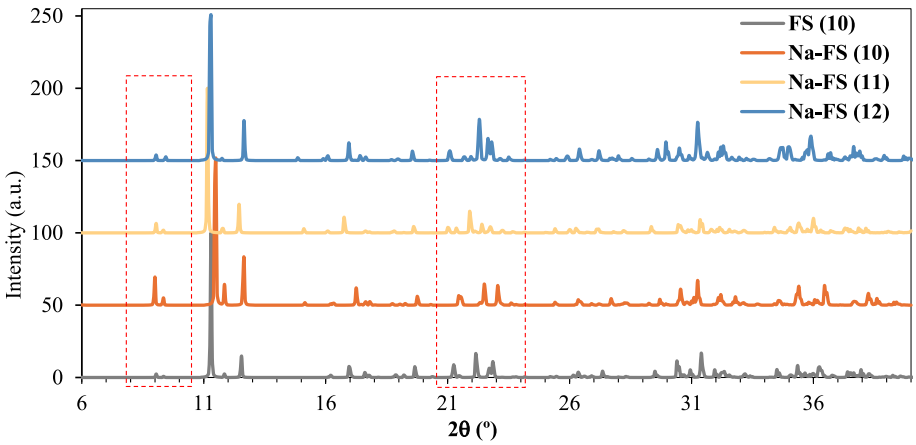

Fig. 7. The computed XRD diffraction peaks of Na-FS.

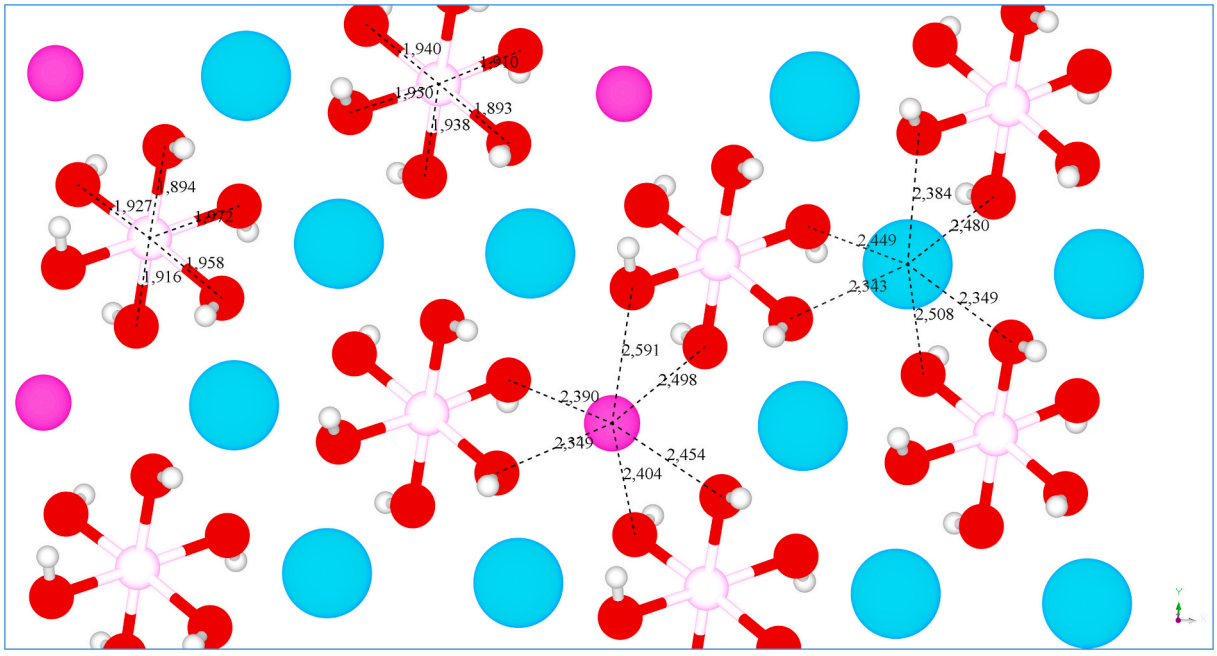

Fig. 8. Visualization of the Al-Ca-OH layer of the minimum energy structure for the Na-FS (11) composition. Na is magenta, Ca is cyan, Al is pink, O is red, and H is white grey. Solid atoms represent the content of the primary unit cell. Distances are given in Å. (For interpretation of the references to colour in this figure legend, the reader is referred to the web version of this article.)

with findings in the experimental work of Georget et al. [19].

The blue series depicts ordinary Portland cement (OPC) systems exposed to chloride-containing solutions of NaCl, $CaCl_2$, and HCl [20]. Results indicate the highest Cl/Al ratio in HCl-exposed samples at a pH of about 10.5, followed by the system exposed to $CaCl_2$ with a pH around 11.7. The study reveals that with HCl and $CaCl_2$ exposure, higher concentrations of the solution led to a greater decrease in pH and consequently, a higher chloride content in FS. However, in the case of the lowest pH obtained in the HCl-exposed series, the Cl content of FS appeared to decrease due to leaching of the AFm. Conversely, exposure to NaCl showed negligible effects on pH or XRD peak shift, with only minor changes observed in the chloride content of FS. Even in this instance, systems with lower chloride content of FS showed a greater peak shift to the higher angle.

Based on these experimental findings, it appears that pH may not be the only determining factor for chloride binding. FS structures with high chloride content can be created in higher pH environments, while lower contents of chloride in FS have also been detected in high pH systems. The cations in solution also play a crucial role, the presence of additional calcium could result in the increase of FS amount, enhancing the chemically bound chlroide content. Additionally, it can increase the chloride concentrationin the diffusion layer of the CASH [42]. The possible cation substitutions in the FS structure by Na^+ typically results in the reduction in chloride binding of structure, which also shifts the diffraction peak to a higher angle when the water molecule numbers remain the same as FS (see Table 4 and Fig. 10b). In a water rich environment, an uptake of one or two more water in the cell structure will create stable hydrogen bond system as shown in Fig. 8 to reduce the total energy, thus stabilizing the cell. The substitution of Ca with Na and additional water will cause a peak shift to the lower angle zone. Ming et al. [44] used ab-initio modelling to reveal the effect of NaCl on AFm structures. They found that chloride ions mainly distributed in the electric double layer of positively charged surface ($[Ca_2Al(OH)_6]^+$) through electrostatic interactions with calcium ions and protons, while sodium ions were mainly confined within the interface region between the negatively charged surface ($[Cl{\cdot}2H_2O]^-$) and hydrocalumite main

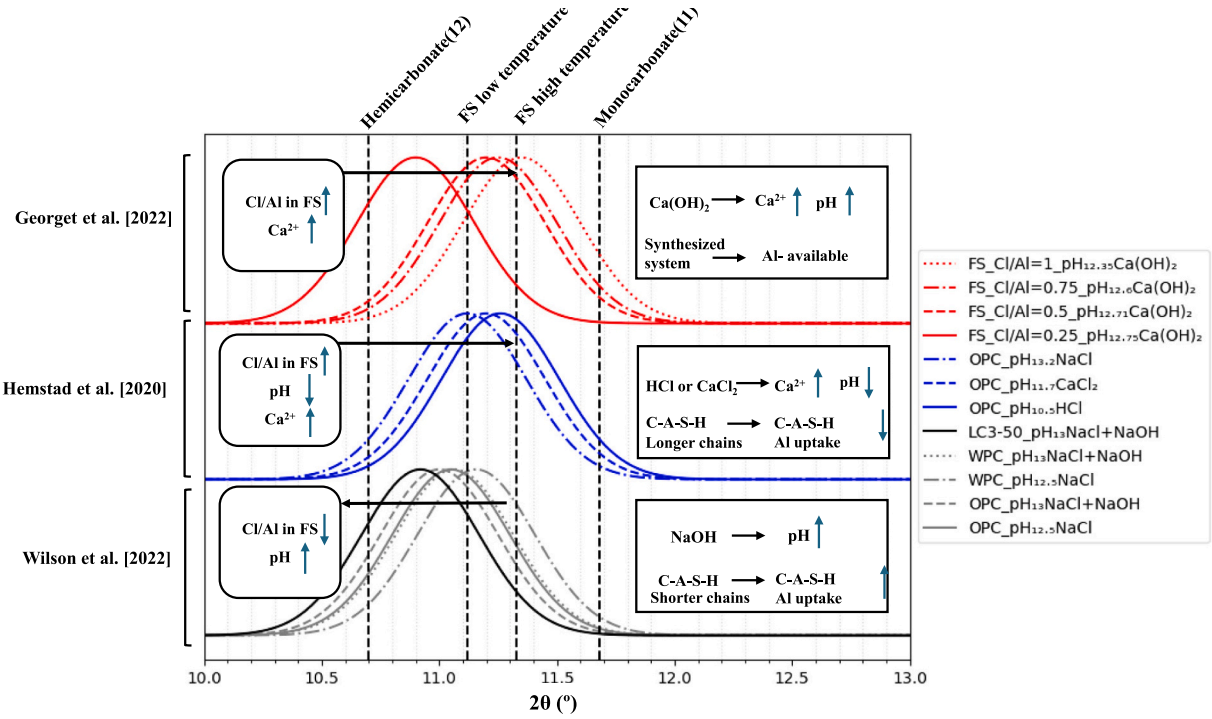

Fig. 9. Correlation between XRD peak shift and chloride content in FS - Experimental data re-plotted from referenced studies [19,20,22,49], the vertical dashed lines represent the location of the XRD peaks for the pure phases of Hemicarbonate (12), low and high temperature FS as well as Monocarbonate (11), showcasing the intricate relationship between pore solution conditions and chloride content in FS. The depicted curves are not exact representations of the data in terms of intensity but are simulated peak positions, designed to provide better visualization and facilitate comparison between the different reported data in literature. For the original data, please refer to the cited references.

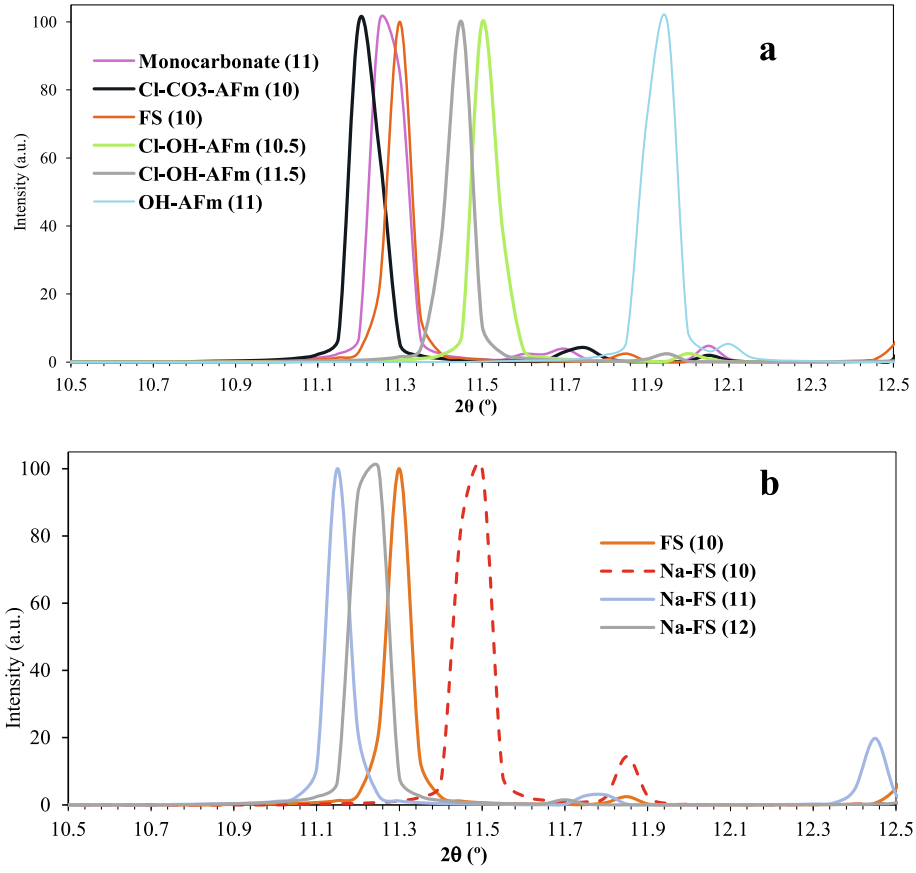

Fig. 10. The modelled shift of diffraction peaks from AFm phases due to the ion substitution in solid solution: a-anion substitution, b-possible cation substitution.

layer, forming various ionic complexes that would probably exists in the solid system. It should be noted that the substitution of Ca by Na in AFm phases is a documented phenomenon, as the U-phase, where sodium is present as $Na(H_2O)_6^+$ oxy-cations in the interlayer. This phase requires an increase in interlayer anions, typically sulfates, for charge compensation [9,30]. However, in our study, the focus is on Na-FS, where sulfates are not considered, therefore, some further experimental research should be carried out to confirm the structure of Na-FS.

For low-carbon binder systems with limestone and carbonation effect, chloride binding is more complex but valuable for modern concrete mixtures. According to Wilson et al., when subjected to NaCl solution, the FS of the LC3–50 (limestone-calcined clay system, with 50% cement substitution) demonstrates the lowest chloride content, and the white cement system unexpectedly exhibits a comparatively high chloride content in its FS [22]. Andrej et al. also found that [45] at higher alkalinity (pH of about 13.5) chloride binding capacities of limestone blended cements are significantly lower if compared with limestone-free cements. It is known to influence mineralogical composition of aluminate phases in a hydrated binder with the CO_3-AFm stabilization. Ming et al. [46] demonstrated that the carbonation process deteriorated the chloride binding capacity of C_3A pastes through producing more calcium mono/hemicarboaluminate phases (Mc/Hc) or forming a solid solution between Mc and Cl-AFm. Shi [47] and Chang [48] stated that AFm phases and Friedel's salt will be carbonated before the portlandite and C-A-S-H to form monocarbonate, thus reducing the chloride binding capacity. It is of great importance to identify the phase changes in the low-carbon binder hydration, especially for FS and mono/hemicarbonate so that the chloride binding capacity can be correctly predicted according to the stoichiometries of crystal structures. A clear understanding of cells with various "Cl-CO_3-OH-H_2O" combinations is the basis for creating quantitative models.

The solid solution $[Ca_2Al(OH)_6]\cdot[Cl_{1-x}\cdot(CO_3)_{x/2}\cdot(2+x/2)\ H_2O]$ in AFm phases was synthesized by Adel et al. [11,12], which confirmed that the existence of Cl-CO_3 hybrid interlayer solid structures. According to our computational results, the substitution of half Cl in the FS with $1/2CO_3^{2-}$ has little effect on the diffraction peaks which is barely detectable by normal XRD measurement (see Fig. 10a). The difference between Cl-CO3-AFm and monocarbonate is also more or less negligible. Therefore, the method of using XRD measurement to evaluate the chemical binding of chloride should be used with care when it comes to the limestone mixed or carbonated system.

5. Concluding remarks

Chloride diffusion determines the durability of reinforced concrete in marine and de-icing environments. A clear understanding of hydrocalumite-like (AFm) phases is significant for the prediction and design of a better chloride binding in sustainable concretes. First-principles computations were performed in this study to assess how ion substitutions affect the cell structure of Friedel's salt. The key findings are summarized as follows:

The optimized crystal structures of $Ca_2Al(OH)_6(Cl,CO_3,OH)\cdot mH_2O$ with various ion substitutions have been established for atomistic modelling. Water plays a critical role in the stability of AFm phases. Varying substitution degrees of chloride with hydroxide ions, likely together with hydration water, is energetically possible and can occur with little change in the unit cell parameters. The flexibility of interlayer hydroxide ions in terms of occupied sites may be a factor for the phase transition of AFm family. The mixing energy change of forming Cl-OH-AFm(10.5) is found to be 20.8 kJ/mol, which implies that the formation of the mixed phase from the pure ones without additional water is energetically unfavorable.

The substitution of half Cl ions in the FS with $1/2CO_3^{2-}$, forming the mixed ions layer, has little effect on the diffraction peaks which is barely detectable by normal XRD measurement. The difference of structure parameter between Cl-CO3-AFm and monocarbonate is also more or less negligible. Therefore, the method of using XRD measurement to evaluate the chemical binding of chloride should be used with more care when it comes to the limestone mixed or carbonated system.

The possible Ca^{2+} substitutions in the FS structure by Na^+ would result in a reduction in chloride binding in the structure, which also shifts the diffraction peak to a larger angle when the water molecule numbers remain the same as FS, but the structure is energetically unstable. In a water-rich environment, the uptake of one or two more water molecules in the structure will stabilize the cell. However, some further experimental research should be carried out to confirm the existence of Na-Friedel's salts structure.

Taken together, these results highlight the need for detailed consideration of interlayer structure. Dynamic simulations of large-scale models, which can give not only structural but also thermodynamic information at finite temperatures, are likely needed to further improve our understanding of the phases and solid solutions that may form. The structures generated in this work are valuable basis for further modelling. While this study focused on the CO_3-Cl-OH system, similar investigations into CO_3-SO_4-OH AFm phases could provide further insights into sulfate incorporation and its impact on chloride binding.

CRediT authorship contribution statement

Liming Huang: Writing – original draft, Visualization, Methodology, Investigation, Formal analysis, Conceptualization. **Erik Bialik:** Writing – original draft, Software, Methodology, Investigation, Data curation, Conceptualization. **Arezou Babaahmadi:** Writing – original draft, Supervision, Project administration, Investigation, Formal analysis, Conceptualization, Funding acquisition.

Declaration of competing interest

We declare that there are no known competing financial interests or personal relationships that could have appeared to influence the work reported in this paper.

Acknowledgements

The authors would like to acknowledge the invaluable support and insightful discussions provided by Prof. Luping Tang and other colleagues in the building materials group at Chalmers.

Appendix A. Supplementary data

Supplementary data to this article can be found online at https://doi.org/10.1016/j.cemconres.2025.107821.

Data availability

Data will be made available on request.

References

[1] L. Tang, D. Boubitsas, L. Huang, Long-term performance of reinforced concrete under a de-icing road environment, Cem. Concr. Res. 164 (2023) 107039.
[2] K. Li, J. Zeng, L. Tang, H.E. Sørensen, C. Andrade, R. Maddalena, L. Huang, G. Geng, P.C. Borges, G.C. Keserle, S. Wang, F. Martirena-Hernández, F. Kanavaris, A.V. Monteiro, K. Kovler, P. Zhang, T. Bansal, T. Visalakshi, R. Torrent, RILEM recommendation from TC 289-DCM: guideline for designing and operating long-term marine exposure sites, Mater. Struct. 57 (2024) 44, https://doi.org/10.1617/s11527-024-02319-9.
[3] M.D.A. Thomas, R.D. Hooton, A. Scott, H. Zibara, The effect of supplementary cementitious materials on chloride binding in hardened cement paste, Cem. Concr. Res. 42 (2012) 1–7, https://doi.org/10.1016/j.cemconres.2011.01.001.
[4] K. De Weerdt, W. Wilson, A. Machner, F. Georget, Chloride profiles – what do they tell us and how should they be used? Cem. Concr. Res. 173 (2023) 107287 https://doi.org/10.1016/j.cemconres.2023.107287.
[5] M. Balonis, Thermodynamic modelling of temperature effects on the mineralogy of Portland cement systems containing chloride, Cem. Concr. Res. 120 (2019) 66–76, https://doi.org/10.1016/j.cemconres.2019.03.011.

[6] M.R. Jones, D.E. Macphee, J.A. Chudek, G. Hunter, R. Lannegrand, R. Talero, S. N. Scrimgeour, Studies using 27Al MAS NMR of AFm and AFt phases and the formation of Friedel's salt, Cem. Concr. Res. 33 (2003) 177–182, https://doi.org/10.1016/S0008-8846(02)00901-8.
[7] S.J. Mills, A.G. Christy, J.-M. Génin, T. Kameda, F. Colombo, Nomenclature of the hydrotalcite supergroup: natural layered double hydroxides, Mineral. Mag. 76 (2012) 1289–1336.
[8] U.A. Birnin-Yauri, F.P. Glasser, Friedel's salt, Ca2Al(OH)6(Cl,OH)·2H2O: its solid solutions and their role in chloride binding, Cem. Concr. Res. 28 (1998) 1713–1723, https://doi.org/10.1016/S0008-8846(98)00162-8.
[9] D. Urushihara, T. Asaka, M. Harada, S. Kondo, M. Nakayama, M. Ogino, E. Owaki, K. Fukuda, Synthesis and structural characterization of U-phase, [3Ca2Al(OH)6][Na(H2O)6(SO4)2·6H2O] layered double hydroxide, J. Solid State Chem. 306 (2022) 122730, https://doi.org/10.1016/j.jssc.2021.122730.
[10] F.P. Glasser, A. Kindness, S.A. Stronach, Stability and solubility relationships in AFm phases part I. Chloride, sulfate and hydroxide, Cem. Concr. Res. 29 (1999) 861–866.
[11] A. Mesbah, J.-P. Rapin, M. François, C. Cau-dit-Coumes, F. Frizon, F. Leroux, G. Renaudin, Crystal structures and phase transition of cementitious bi-anionic AFm-(cl−, CO32−) compounds: crystal structures and phase transition, J. Am. Ceram. Soc. 94 (2011) 261–268, https://doi.org/10.1111/j.1551-2916.2010.04050.x.
[12] A. Mesbah, C. Cau-dit-Coumes, F. Frizon, F. Leroux, J. Ravaux, G. Renaudin, A new investigation of the cl−-CO32− substitution in AFm phases: a new investigation of the cl−-CO32− substitution in AFm phases, J. Am. Ceram. Soc. 94 (2011) 1901–1910, https://doi.org/10.1111/j.1551-2916.2010.04305.x.
[13] A.K. Suryavanshi, R. Narayan Swamy, Stability of Friedel's salt in carbonated concrete structural elements, Cem. Concr. Res. 26 (1996) 729–741, https://doi.org/10.1016/S0008-8846(96)85010-1.
[14] J.-P. Rapin, G. Renaudin, E. Elkaim, M. Francois, Structural transition of Friedel's salt 3CaO· Al2O3· CaCl2· 10H2O studied by synchrotron powder diffraction, Cem. Concr. Res. 32 (2002) 513–519.
[15] M.D. Andersen, H.J. Jakobsen, J. Skibsted, Characterization of the α− β phase transition in Friedels salt (Ca2Al (OH) 6Cl⊙ 2H2O) by variable-temperature 27Al MAS NMR spectroscopy, Chem. A Eur. J. 106 (2002) 6676–6682.
[16] M.C. Dalconi, G. Artioli, N. Masciocchi, C. Giacobbe, F. Castiglioni, G. Ferrari, The crystal structure of a new calcium aluminate phase containing formate, Cem. Concr. Res. 146 (2021) 106490, https://doi.org/10.1016/j.cemconres.2021.106490.
[17] L. Vieille, I. Rousselot, F. Leroux, J.-P. Besse, C. Taviot-Guého, Hydrocalumite and its polymer derivatives. 1. Reversible thermal behavior of Friedel's salt: a direct observation by means of high-temperature in situ powder X-ray diffraction, Chem. Mater. 15 (2003) 4361–4368.
[18] R. Talero, L. Trusilewicz, A. Delgado, C. Pedrajas, R. Lannegrand, V. Rahhal, R. Mejía, S. Delvasto, F.A. Ramírez, Comparative and semi-quantitative XRD analysis of Friedel's salt originating from pozzolan and Portland cement, Construct. Build Mater. 25 (2011) 2370–2380, https://doi.org/10.1016/j.conbuildmat.2010.11.037.
[19] F. Georget, B. Lothenbach, W. Wilson, F. Zunino, K.L. Scrivener, Stability of hemicarbonate under cement paste-like conditions, Cem. Concr. Res. 153 (2022) 106692, https://doi.org/10.1016/j.cemconres.2021.106692.
[20] P. Hemstad, A. Machner, K. De Weerdt, The effect of artificial leaching with HCl on chloride binding in ordinary Portland cement paste, Cem. Concr. Res. 130 (2020) 105976, https://doi.org/10.1016/j.cemconres.2020.105976.
[21] F. Avet, K. Scrivener, Influence of pH on the chloride binding capacity of limestone calcined clay cements (LC3), Cem. Concr. Res. 131 (2020) 106031, https://doi.org/10.1016/j.cemconres.2020.106031.
[22] W. Wilson, J.N. Gonthier, F. Georget, K.L. Scrivener, Insights on chemical and physical chloride binding in blended cement pastes, Cem. Concr. Res. 156 (2022) 106747, https://doi.org/10.1016/j.cemconres.2022.106747.
[23] J.D. Head, M.C. Zerner, A Broyden—fletcher—Goldfarb—Shanno optimization procedure for molecular geometries, Chem. Phys. Lett. 122 (1985) 264–270.
[24] J.P. Perdew, K. Burke, M. Ernzerhof, Generalized gradient approximation made simple, Phys. Rev. Lett. 77 (1996) 3865.
[25] S. Grimme, J. Antony, S. Ehrlich, H. Krieg, A consistent and accurate ab initio parametrization of density functional dispersion correction (DFT-D) for the 94 elements H-Pu, J. Chem. Phys. 132 (2010).
[26] V. Kostal, P.E. Mason, H. Martinez-Seara, P. Jungwirth, Common cations are not polarizable: effects of dispersion correction on hydration structures from ab initio molecular dynamics, J. Phys. Chem. Lett. 14 (2023) 4403–4408.
[27] S. Goedecker, M. Teter, J. Hutter, Separable dual-space Gaussian pseudopotentials, Phys. Rev. B 54 (1996) 1703.
[28] T.D. Kühne, M. Iannuzzi, M. Del Ben, V.V. Rybkin, P. Seewald, F. Stein, T. Laino, R. Z. Khaliullin, O. Schütt, F. Schiffmann, CP2K: an electronic structure and molecular dynamics software package-quickstep: efficient and accurate electronic structure calculations, J. Chem. Phys. 152 (2020).
[29] A. Mesbah, M. François, C. Cau-dit-Coumes, F. Frizon, Y. Filinchuk, F. Leroux, J. Ravaux, G. Renaudin, Crystal structure of Kuzel's salt 3CaO·Al2O3·1/2CaSO4·1/2CaCl2·11H2O determined by synchrotron powder diffraction, Cem. Concr. Res. 41 (2011) 504–509, https://doi.org/10.1016/j.cemconres.2011.01.015.
[30] W. Dosch, H., Zur Strassen, Ein alkalihaltiges Calciumaluminatsulfathydrat (Natrium-Monosulfat), Zement-Kalk-Gips 9 (1967) 392–401.
[31] K.M. Flurchick, DFT functionals and molecular geometries, Chem. Phys. Lett. 421 (2006) 540–543, https://doi.org/10.1016/j.cplett.2006.01.112.
[32] P. Wernet, D. Nordlund, U. Bergmann, M. Cavalleri, M. Odelius, H. Ogasawara, L. A. Naslund, T.K. Hirsch, L. Ojamae, P. Glatzel, The structure of the first coordination shell in liquid water, Science 304 (2004) 995–999.
[33] F.N. Keutsch, R.J. Saykally, Water clusters: untangling the mysteries of the liquid, one molecule at a time, Proc. Natl. Acad. Sci. U. S. A. 98 (2001) 10533–10540, https://doi.org/10.1073/pnas.191266498.
[34] M. Sacerdoti, E. Passaglia, Hydrocalumite from Latium, Italy: its crystal structure and relationship with related synthetic phases, Neues Jb. Mineral. Monat. (1988) 462–475.
[35] T. Honorio, Monocarboluminate: sorption dependence of thermal, elastic, and transport properties, J. Am. Ceram. Soc. (2024) e20246, https://doi.org/10.1111/jace.20246.
[36] M. Balonis, B. Lothenbach, G. Le Saout, F.P. Glasser, Impact of chloride on the mineralogy of hydrated Portland cement systems, Cem. Concr. Res. 40 (2010) 1009–1022, https://doi.org/10.1016/j.cemconres.2010.03.002.
[37] F.H. Stillinger, Water revisited, Science 209 (1980) 451–457.
[38] S. Ansell, A.C. Barnes, P.E. Mason, G.W. Neilson, S. Ramos, X-ray and neutron scattering studies of the hydration structure of alkali ions in concentrated aqueous solutions, Biophys. Chem. 124 (2006) 171–179.
[39] A. Babaahmadi, A. Machner, W. Kunther, J. Figueira, P. Hemstad, K. De Weerdt, Chloride binding in Portland composite cements containing metakaolin and silica fume, Cem. Concr. Res. 161 (2022) 106924.
[40] A. Babaahmadi, L. Tang, Z. Abbas, T. Zack, P. Mårtensson, Development of an electro-chemical accelerated ageing method for leaching of calcium from cementitious materials, Mater. Struct. 49 (2016) 705–718.
[41] E. L'hôpital, B. Lothenbach, G. Le Saout, D. Kulik, K. Scrivener, Incorporation of aluminium in calcium-silicate-hydrates, Cem. Concr. Res. 75 (2015) 91–103.
[42] Z. Shi, M.R. Geiker, K. De Weerdt, T.A. Østnor, B. Lothenbach, F. Winnefeld, J. Skibsted, Role of calcium on chloride binding in hydrated Portland cement–metakaolin–limestone blends, Cem. Concr. Res. 95 (2017) 205–216, https://doi.org/10.1016/j.cemconres.2017.02.003.
[43] C.A.J. Appelo, The anion exchange properties of AFm (hydrocalumite-group) minerals defined from solubility experiments and crystallographic information, Cem. Concr. Res. 140 (2021) 106270, https://doi.org/10.1016/j.cemconres.2020.106270.
[44] X. Ming, Q. Liu, Y. Li, Y. Cai, Z. Li, Ab-initio modeling of chloride binding at hydrocalumite/sodium chloride solution interfaces, Cem. Concr. Res. 162 (2022) 106996, https://doi.org/10.1016/j.cemconres.2022.106996.
[45] A. Ipavec, T. Vuk, R. Gabrovšek, V. Kaučič, Chloride binding into hydrated blended cements: the influence of limestone and alkalinity, Cem. Concr. Res. 48 (2013) 74–85, https://doi.org/10.1016/j.cemconres.2013.02.010.
[46] X. Ming, Y. Li, Q. Liu, M. Wang, Y. Cai, B. Chen, Z. Li, Chloride binding behaviors and early age hydration of tricalcium aluminate in chloride-containing solutions, Cem. Concr. Compos. 137 (2023) 104928, https://doi.org/10.1016/j.cemconcomp.2023.104928.
[47] Z. Shi, B. Lothenbach, M.R. Geiker, J. Kaufmann, A. Leemann, S. Ferreiro, J. Skibsted, Experimental studies and thermodynamic modeling of the carbonation of Portland cement, metakaolin and limestone mortars, Cem. Concr. Res. 88 (2016) 60–72, https://doi.org/10.1016/j.cemconres.2016.06.006.
[48] H. Chang, Chloride binding capacity of pastes influenced by carbonation under three conditions, Cem. Concr. Compos. 84 (2017) 1–9, https://doi.org/10.1016/j.cemconcomp.2017.08.011.
[49] W. Wilson, J.N. Gonthier, F. Georget, K.L. Scrivener, Dataset: Insights on chemical and physical chloride binding in blended-cement pastes, Zenodo (2022), https://doi.org/10.5281/zenodo.6288426.